Mikrochim. Acta 119, 1–12 (1995)

Mikrochimica Acta

Classification of Secondary Ion Mass Spectrometry (SIMS) Micrographs to Characterize Chemical Phases

Christopher Latkoczy[1], Herbert Hutter[1,*], Manfred Grasserbauer[1], and Peter Wilhartitz[2]

[1] Institute for Analytical Chemistry, Vienna University of Technology, Getreidemarkt 9/151, A-1060 Vienna, Austria

[2] Metallwerk Plansee GmbH, A-6600 Reutte/Tirol, Austria

Abstract. This work demonstrates the potential of multivariate image analysis methods in the extraction of useful, problem dependent information from SIMS images. Specific algorithms have been developed to classify SIMS micrographs manually as well as automatically. A feature selection has been achieved by means of principal component analysis with a subsequent image classification.

As an application example for these improved digital image processing tools chemical phases within a soldered industrial metal sample have been identified. This is of highly practical value as it was assumed that during the soldering process inhomogeneities occur along the joint site which cause a cracking of the brazed material under mechanical strain conditions.

Key words: secondary ion mass spectrometry (SIMS), imaging, classification, principal component analysis (PCA).

Digital image analysis, initially developed in the sixties for exploration purposes, has spread as a new powerful tool over a whole variety of disciplines. Physical dimensions do not set any limits to its application possibilities: ranging from satellite based sensing in space, down to the atomic level of scanning tunneling microscopy [1], digital image processing techniques are now extensively employed. They have also proved to be very attractive for chemical analytical aims where they provide the advantage of visualization of data otherwise difficult to grasp, for example because of very large data sets, and also the advantage of possible quantification of purely optical, qualitative information. The digitized images used for such operations are statistical to the core because a numerical value can be allocated to each to their pixels and therefore they obviously contain more information than mere size or shape. Digital image processing techniques applied to such micrographs directly induce a calculation of the underlying data. Vice versa, statistical operations within

* To whom correspondence should be addressed

the data set automatically result in altered graphic representations for each calculation.

There are several major analytical techniques, which are capable of producing an image. These include optical microscopy [2], electron microscopy (EPMA) [3–6], ion microscopy (as used in secondary ion mass spectrometry (SIMS)) [7–10], X-ray and NMR tomography [11, 12]. Univariate operations for reducing noise and enhancing the image quality can be carried out on the pictures obtained before submitting them to further multivariate analysis [13]. In this investigation the images were acquired with SIMS and then analyzed to identify chemical phases within a metal sample. This new application of digital image processing will not only be useful in solving problems in materials science (as described below), but, using the programmed interface together with the developed half-automatic step-by-step analysis here, digital image processing shows much promise as a valuable interactive tool in related areas of analysis, e.g. to classify EPMA maps.

Experimental

Sample Description

Amorphous and microcrystalline filler metals are currently used in a wide variety of brazing and soldering applications. These materials are typically cast to a foil form for direct use in metal joining. Brazing and soldering are processes for joining metals through the creation of a permanent metallurgical bond. The joining process is accomplished by inductively heating the assembly and adding a filler metal that must exhibit a liquidus temperature lower than the solidus temperature of the base metals. As the assembly is allowed to cool, the filler solidifies forming metallurgical bonds with the mating base metal surfaces. The thermal cycle in the joining process must be such that the filler metal is melted but the base metals are neither melted nor undesirably annealed or distorted. The interaction between the molten filler metal and the solid base materials must also promote wetting, in which the molten filler metal spreads and adheres to the surface of the base material. Finally, the solidified joint must provide sufficient mechanical stability for the intended use. However, effects such as the interdiffusion of components between the molten filler metal and the base material, especially the dissolution of the base material in the filler metal, sometimes occur. The final assembly then may exhibit undesirable crevices and therefore may not satisfy the industrial requirements.

This was the case for the sample analyzed here. The analyzed sample was a X-ray anode consisting of a brazed joint between a highly alloyed steel and high purity chromium. A nickel base alloy in form of a foil was used as the filler metal. Its composition was: 82.5 at % Ni, 7 at % Cr, 4.5 at % Si, 3 at % B and 3 at % Fe, with boron and silicon acting as melting depressors. The material is homogeneous, i.e. it does not contain other phases before the brazing process. During brazing cracks developed, which were obviously caused by the formation of brittle phases.

It was the aim of these investigations to detect, localize and classify these brittle phases within the foil and its neighboring surfaces. For the analytical investigation a polished cross section was prepared. The thickness of the brazing seam was about 200 μm. The diameter of the area used for imaging SIMS was 400 μm (see Fig. 1).

Imaging SIMS

Properties in the solid state originate not only from the chemical composition but also from the degree of chemical heterogeneity. For the study of material homogeneity ion microscopy is a powerful tool due to its capability for chemical imaging [14].

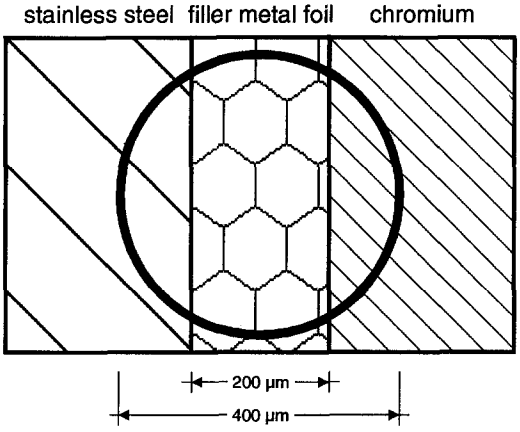

Fig. 1. Schematic representation of the analyzed sample

For this work, α CAMECA IMS-3f ion microscope was used. A mass filtered 2µA O_2^+ intensive primary ion beam was focused on the sample scanning an area of 500 × 500 µm to obtain an analyzed area of 400 µm in diameter. The secondary ion fraction of the sputtered material was then accelerated into a double focussing mass spectrometer with a resolution of $M/\Delta M = 300$ for mass selection. A double microchannel plate (GALILEO CHEVRON HOT MCP™) with a gain of 10^6 was used to convert the ions to electrons which were then projected onto a fluorescent screen, to be viewed with a charge coupled device (CCD) camera system (Pulnix™ 700). This camera transformed the incoming light signals of the phosphorus screen to analogue signals with a resolution of 786 × 586 pixel (dimensions 11 × 11 µm²) and a light sensitivity of 0.5 lux. These analog signals were directed to an image processor (IMAGING TECHNOLOGY INTERNATIONAL 151) to be digitized and displayed for further image processing techniques. Synchronization of all signals was made possible by computer control using a PC (HP Vectra 486, 66 MHz, 8 MB RAM, 700 MB harddisk 2.2 GB backup tape) [15]. Due to the fact that the applied secondary optical system is stigmatic, a one-to-one mapping of the original position of the atoms in the sample was preserved in the acquired and stored image.

As the sample consisted of many different components (highly alloyed steel, chromium, mixed phases inside the brazing foil), the resulting mass spectra were very complex. While atomic signals (B^+, Si^+, Cr^+, Fe^+, Ni^+), gave clear peaks, the signals of cluster ions often showed peak interferences. The traditional way of avoiding such interferences is to increase mass resolution, but this also leads to a lower lateral resolution of the secondary ion image and therefore results in a loss of information. In this work these difficulties were overcome by keeping the mass resolution low, and then applying multivariate statistical methods on the image of gain clear information about all atomic signals, as well as all cluster ions signals.

The following ions were selected out of the low mass resolution spectrum as they represent the major combinations of the compounds of the sample:

11: B^+	28: Si^+	39: SiB^+	52: Cr^+
56: Fe^+	58: Ni^+	63: CrB^+	67: FeB^+
69: NiB^+	80: $CrSi^+$	84: $FeSi^+$	86: $NiSi^+$

Micrographs of the chosen masses were assigned to elements and clusters and possible peak interferences were not considered (see Fig. 2).

To reduce the non-linearities of the channel plate all distributions were picked up with one and the same channel plate voltage. This has been done by reducing the primary ion beam intensity so that all secondary ion intensities are in the single ion counting range of the channel plate. In order to receive a sufficiently high signal-to-noise ratio different summing up times were used. The distributions were

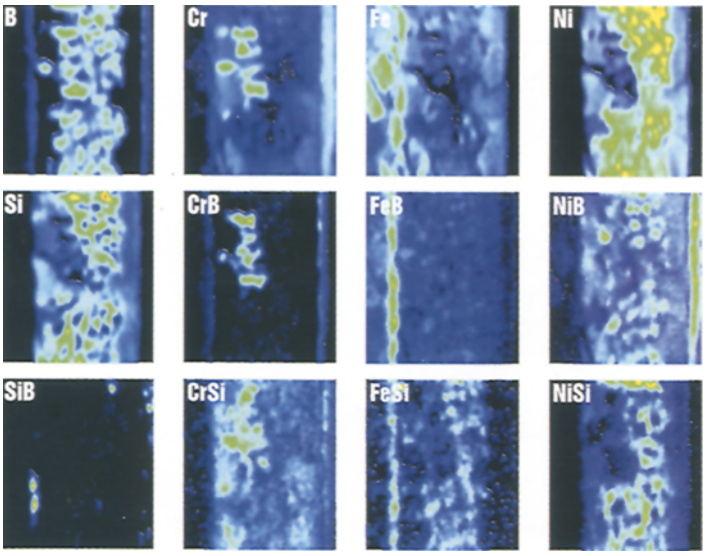

Fig. 2. Original SIMS micrographs of sample (270 × 300 µm, stored in 256 × 256 Pixels, 8bit)

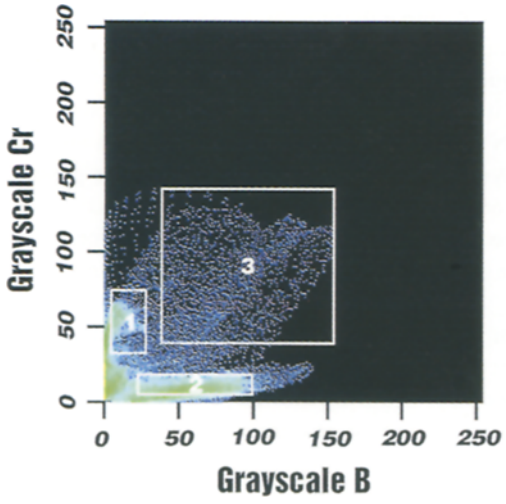

Fig. 4a. Two dimensional scatter diagram for the B- and Cr-SIMS map (with rectangles according to single pixel clusters)

Fig. 4b. Classified image achieved from the manual classification of the B- and Cr-SIMS map

scaled and stored as 8-bit Windows BMP files. This does not affect the results of the classification, since we are interested only in the relative intensities of the images.

Image Classification

In a digital map of secondary ion distributions, numerical data are encoded in each of the picture's elements containing positional as well as chemical information. Chemical and geometric features (like texture, shape) in the SIMS micrographs lead

to pixel populations in coherent clusters and can therefore be treated further, by multivariate statistical means to extract analytical information, e.g. image segmentation for correlation of positional data can be performed [16].

A further step is then a classification of the specific chemical features contained in the sample: to identify different objects in this features space, it is necessary to establish their frequency distribution. Different classification strategies are possible: supervised, non-supervised, supervised learning and non-supervised learning classification strategies [17, 18]. The resulting clusters ideally represent the relationship of the constituents in the original sample. Within the digital grayscale mappings (covering a range of 0–255, representing the secondary ion intensities), single picture objects differ in their gray levels according to the chemical phases of the original sample. The numerical concentration information for each pixel deduced from these gray level clusters can then be displayed in mathematical and graphical models. The grouping of each picture element to one of the depicted objects was not known in advance. Each picture element could be assigned to an object employing a classification strategy: in this case a so called 'minimum-distance-cluster algorithm' was employed.

As the mathematical mode of display a scatter plot was used for this investigation. It was calculated to represent the frequency distribution of gray levels, which point out the position of the objects (phases) in two dimensional space [19–23]. Scatter plots for three dimensional space can also be graphically acquired [24], but little additional information is thereby gained and the increased programming expenses are not justified. It was found that for the problem investigated a two dimensional scatter plot revealed sufficient information. Figure 3 demonstrates the construction principle for such scatter plots. A lot of pixels in these diagrams tend to pile up at the same spots as they possess the same relative frequency distribution of gray levels in both images. To achieve a clearer visualization of single picture units, the plot was treated with a pseudo logarithmic density color scale. These colored plots allowed a determination of pixel clusters (representing single sample phases), outliers and gradients in terms of their density. To split the resulting picture clusters (according to their phase of origin) during classification, a rectangle was manually positioned on the screen with the mouse to outline single pixel clusters (see Fig. 4a).

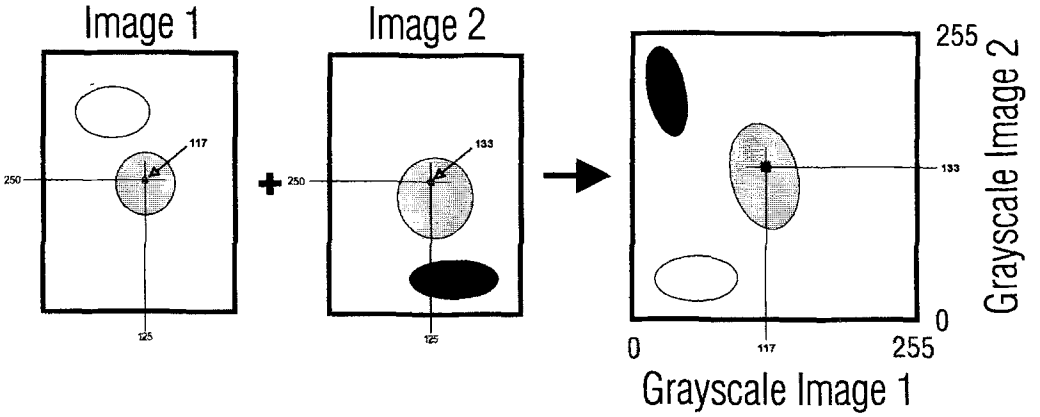

Fig. 3. Construction principle of a two dimensional scatter diagram. Numbers are pixel intensities (grayscale values)

Because these pixel clusters were selected by hand this special classification strategy will be called 'manual classification'. Picture elements within the rectangle were numerically backprojected onto the original SIMS maps. The established matching regions of the same gray level distribution were colored and displayed in a new classified image (see Fig. 4b).

Now different chemical phases of the sample could be identified and localized when comparing the classified image (see Fig. 4b) with the three original SIMS maps for B, Cr and CrB (see Fig. 2): clusters with a high gray level (representing the secondary ion intensity) for Cr and simultaneously a low gray level for B (region 1) originate from the chromium-phase. High gray levels for B and low values for Cr (region 2) indicate a boride-phase, whereas similar gray levels for both elements (region 3) characterize the chromium boride-phase. The obvious advantage of these procedures lies in an apparent identification of mixed chemical phases.

The advantage of image classification for the identification and localization of phases over the alternative technique, namely imaging of cluster ions being representative for such a phase (e.g. CrB^+) is evident for cases when these cluster ions are disturbed by interferences. This is rather often the case for multicomponent systems, e.g. in case of the solder system the mass of 68 could represent either the $^{57}Fe\ ^{11}B$ phase or the $^{58}Ni\ ^{10}B$ phase.

This manual classification strategy can no longer be applied if a classification of more than two images is required: therefore an automatic classification algorithm was developed for the multidimensional case. This algorithm assigns neighboring pixels of the multidimensional score plot to the same class. The Euclidean distance was used as a measure between these pixels [25]. For a grouping of the pixels, so called class centers must first be defined. Any feature vector, or pixel of the n-dimensional feature space, can be assigned to represent a first class center. Then all the other feature vectors can be assigned to this established first class center, as long as the previously defined distance criteria are met. When a feature vector exceeds a given threshold this vector itself establishes a new class center. Proceeding in this manner all class centers can be found. For the remaining vectors the respective distances to all class centers have to be calculated in order to assign them to that previously found class to which their Euclidean distance was the shortest. The resulting classes build up the two-dimensional scatter diagram for automatic classification and can be emphasized by differential coloring. As in the case of manual classification they can again be projected back upon the original SIMS images to obtain the classified image.

The whole program to calculate and display the scatter diagram, to outline single clusters and to display and to color the classified image was established and programmed in our group. The programming language used was Microsoft C^{++}. In the case of automatic classification the commonly used minimum-distance-cluster algorithm was adopted and substantially improved.

It can be observed that comparable results were obtained with automatic and manual classification, but automatic classification has the advantage of enabling the classification of more than two images, which is often required. To demonstrate this, five (B, Cr, Fe, Ni, Si) SIMS images were classified. But as one can see, the necessary comparison with the original SIMS mappings to identify the chemical phases becomes rather difficult and an exact matching is nearly impossible (see Fig. 5).

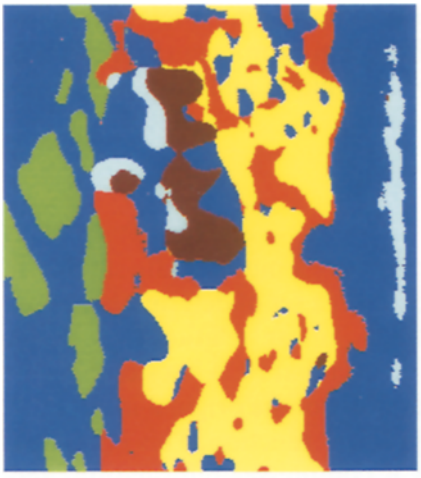

Fig. 5. Classified image acquired from the automatic classification of the B-, the Cr-, Fe-, the Ni- and Si-SIMS map (Threshold: 110)

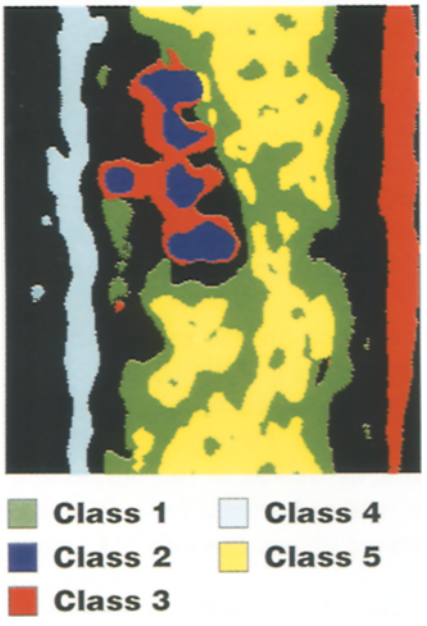

Fig. 8. Automatic classification of the first three principal components (Threshold: 75)

Automatic classification also has two main disadvantages: firstly, chosen thresholds affect the classification results in a decisive manner. A threshold value set too high falsely assigns more than one chemical phase to a single class, whereas a threshold value that is too low splits up a chemical phase actually belonging to only one class. The proper value of the threshold can not be known in advance but a threshold value of about 100 has proven to give the best results when comparing the different classified images with the original SIMS micrographs. Secondly, the more pictures that are brought in for classification, the more difficult the necessary comparison with the original SIMS mappings becomes. A compression of the information contained in all micrographs into some main channels is one possibility to overcome interpretation difficulties. A successful classification can then be restricted to these channels.

For such an approach an objective means for selection of most relevant information from the SIMS micrographs is required. Principal component analysis was chosen as a data reduction and feature selection technique and combined with subsequent image classification.

Principal Component Analysis

Principal component analysis (PCA) may only be used as a multivariate statistical tool when all experimental data are solely dependent on a set of determining parameters and the experimental data exhibit a strictly linear relationship to the determining parameters [26]. This is derived from the fact that PCA is a step-by-step linear transformation of data, in which the raw variables of the original images are successively transformed into latent variables by a linear function. This operation determines the influence parameters in so far as it compresses information, and results in the so called 'principal components' of the original images. The principal components are linearly independent, uncorrelated in pairs and sorted by their variance value. This results in a compression of the overall variance within the data set to the first principal components. Further, although the overall signal-to-noise ratio remains unchanged as a result of the transformation, the first principal components are the least noisy and the last ones are the noisiest. During analysis, the last principal components can therefore be neglected without loss of information. These properties are useful, not only to reduce the amount of data that has to be stored and handled, but one can restrict the further classification to the first principal components.

In the present case, the influence exerting parameters are the main chemical phases (Ni, Cr, Si, B, Fe) of the sample, and all mixed phases (e.g. SiB, CrB, FeSi, NiSi) a mere linear combination of them. Constituents of the mixed chemical phases may appear in different mappings of secondary ion distributions. The chromium boride phase is, for example, represented in the chromium, as well as in the boride and chromium boride secondary ion micrograph. The required criteria for a PCA are met by the fact that the metallic bond making in mixed phases can only take place with linear combinations of their constituents.

Although commercial software packages are available (usually comprised in statistical libraries such as SPSS), a problem-specific software was specially developed and programmed in our group to perform the principal component analysis. The programmed algorithm (programming language used was Microsoft C^{++})

1. calculates the covariance matrix of the image set. If N images are given, this covariance matrix is a $N \times N$ matrix of cross-correlation and autocorrelation coefficients. A high coefficient means a high correlation between two images. A coefficient of zero stands for no correlation, and a coefficient of less than zero signifies anti-correlation,
2. finds the eigenvalues and eigenvectors of the covariance matrix in a next step,
3. sorts these eigenvectors by size of their eigenvalues into rows in a new $N \times N$ matrix in which the eigenvector corresponding to the largest eigenvalue forms the first row, and that eigenvector corresponding to the smallest eigenvalues forms the last row,

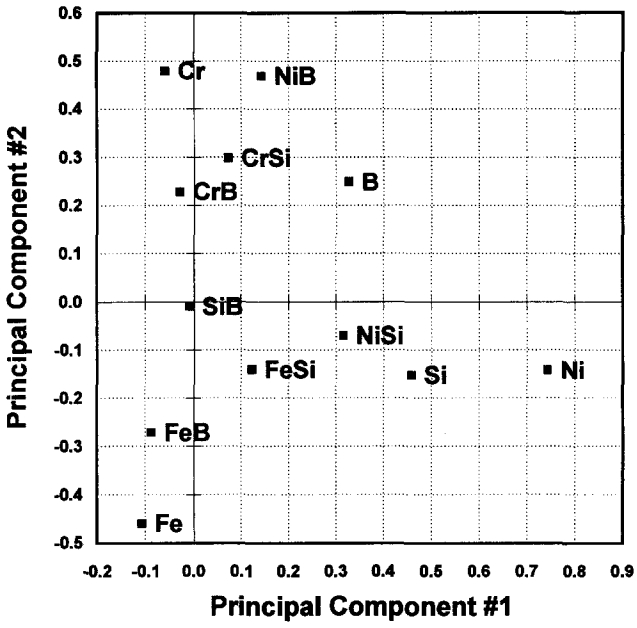

Fig. 6. Loading plot of the first and second principal component

4. finally multiplies the raw images with this 'eigenvector matrix' in order to acquire the set of principal components of the original images.

The pictorial effect of the algorithm consists of a rotation of the scatter plot so as to place the direction of greatest variance along one axis and to generate the set of orthonormal principal components. In image processing language this means that PCA images are maximally different from each other.

The numerical values of the eigenvectors are called 'loading factors' and can be displayed in a 'loading plot' [27]. These factor express the influence of single SIMS maps on the principal components (see Fig. 6). From the loading plots preliminary information about those chemical phases influencing the classified image can be drawn. The value of the loading factors also gives an indication which principal

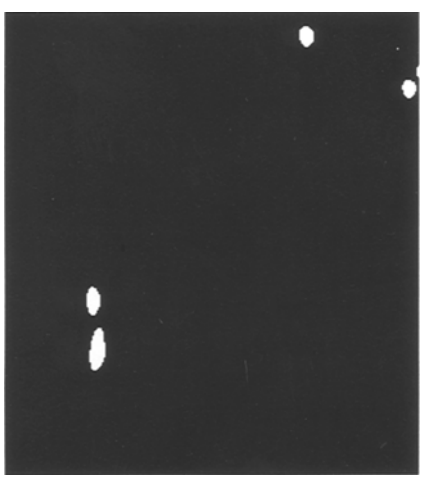

Fig. 7. Classified image achieved from the tenth and eleventh principal component to obtain the SiB-phase

Table 1. Eigenvalues expressed as percentage of the sum of squares for the principal component analysis

PC#	% Sum of squares	% Sum of squares cumulative
1	48.802	48.8
2	15.279	64.1
3	8.758	72.8
4	6.557	79.4
5	6.372	85.8
6	4.257	90.0
7	3.154	93.2
8	2.329	95.2
9	1.573	97.1
10	1.168	98.2
11	1.053	99.3
12	0.699	100.0

components must be classified to identify a typical phase. Figure 7 exemplifies this fact: the tenth and eleventh principal components were classified. The values for the loading factors were both high for silicon boride which led to a definitive identification of the silicon boride phase (compare the SiB SIMS micrograph in Fig. 2).

Classification of the principal components can be achieved by either manually positioning rectangles to choose clusters, or by automatic calculation with the classification algorithm. In order to cover the whole range of gray levels in the scatter plot, the mean gray level value of the principal components was shifted to 127 and the variances multiplied with a scaling factor of 0.7. As the principal components are only a different numerical representation of the original SIMS images, a mathematical transformation can be defined that matches either manually or automatically selected areas of the classified image with corresponding gray levels in the original SIMS micrographs. The value of the gray levels found, indicate the respective influence of each SIMS map on different regions within the classified image. Therefore it was possible to identify the phases occurring in the sample.

In fact, the numerical values of the calculated gray levels did not precisely match to the exact gray level values of the SIMS images. The reason is that the single principal components include only a certain percentage of the total sum of squares, which can be understood as the percentage of the total information content given in the original SIMS maps, as the eigenvalues represent the expected values for the principal component variances (see Table 1). A directional trend nevertheless can be observed which allows a qualitatively correct interpretation of given regions within the classified image. In a classification example of the three initial principle components that embody 72.8% of the total sum of squares, the main chemical phases of the sample was successfully identified. In this case class 1 indicates the nickel silicide phase, class 2 the chromium boride phase, class 3 the chromium phase, class 4 the iron boride phase and class 5 the nickel boride phase (see Fig. 8 and Table 2).

Table 2. Computed gray levels of the five classes found when classifying the first three principal components

Class	B	Cr	CrB	CrSi	Fe	FeB	FeSi	Ni	NiB	NiSi	Si	SiB
1	42	0	0	0	0	0	2	54	0	77	45	0
2	65	59	75	32	0	0	0	0	40	0	0	0
3	39	162	48	37	0	4	7	2	25	0	0	1
4	69	0	9	0	71	82	38	0	0	0	0	2
5	122	3	11	17	0	12	40	124	150	44	43	0

Results and Discussion

This work demonstrates the use of principal component analysis with a subsequent classification in image analysis for chemical phase detection. The above detected brittle boride and silicide phases turned out to be responsible for the cracking of the metallic sample under mechanical strain.

In addition, the minimizing of data handling during principal component analysis has been shown. The classification results strongly depend on the number of principal components used: the most exact separation of phases is to be expected when classifying all principal components. For practical classification purposes, nevertheless, adequate results have been obtained by using the data of only the main principal components. However, it is important to take a cautious approach, as outliers and artifacts tend to accumulate in the last principal components (refer to the identification process of the silicon boride phase, which could not be determined until the tenth and eleventh principal components had been classified). A manual classification of two pictures can provide a first impression of a sample situation, whereas an automatic classification has proven to be suitable for more than two pictures.

The exact stoichiometry of the given phases in the sample could not be determined and therefore their true identity remains open. Neighboring submicron phases could not be resolved and might have influenced the identification. Furthermore, mixed MeSiB phases have not been considered in this work.

This example of PCA with subsequent classification is not restricted to imaging SIMS measurements alone, but can be applied to any analytical imaging method. The use of specialized classification algorithms in the future, promises further developments in this field. With further specialization of classification algorithms, for example with neural networks, the method can be further expanded into an even more powerful analytical tool.

Acknowledgement. The authors thank Kurt Piplits for his valuable contributions operating the SIMS hardware and making SIMS measurements. Thanks also go to Katarina Matiasek for countless conversations in which ideas in this article took shape.

Credit. The authors wish to thank the Austrian Scientific Research Council (project S 6205), and the Austrian Industrial Research Council (project 2/293) for the financial support provided.

References

[1] D. S. Mantus, G. H. Morrison, *J. Vac. Sci. Technol.* **1990**, *A8*, 2209.
[2] R. Cooke, *Anal. Chem.* **1990**, *62*, 423R.
[3] C. Fiori, *Anal. Chem.* **1988**, *60*, 86R.
[4] P. Geladi, K. Esbensen, *J. Chemom.* **1989**, *3*, 419.
[5] R. Barer, V. Cosslett (eds.), *Adv. Opt. Electron Microsc., Vol. 10*, Academic Press, London 1987.
[6] T. Mulvey, C. Sheppard (eds.), *Adv. Opt. Electron Microsc., Vol 11*, Academic Press, London 1988.
[7] H. E. Bishop, *Electron Microsc. Anal.* **1987**, 51–56.
[8] J. L. Hunter Jr., S. F. Corcoran, R. W. Linton, D. P. Griffis, *Microbeam Anal.* **1989**, *24*, 597.
[9] R. W. Linton, J. J. Lee, J. L. Hunter Jr., J. D. Shelburne, in: *Secondary Ion Mass Spectrometry (SIMS VII)* (A. Benninghoven, C. A. Evans, K. D. McKeegan, H. A. Storms, H. W. Werner, eds.) Wiley, New York, 1990, pp. 331–334.
[10] J. L. Hunter Jr., R. W. Linton, D. P. Griffis, *J. Vac. Sci. Technol.* **1991**, *A9*, 1622.
[11] G. Nesbitt, A. de Groot, *Trends Anal. Chem.* **1990**, *9*, 263.
[12] J. Miller, *Trends Anal. Chem.* **1991**, *10*, 59.
[13] P. Geladi, E. Bengtsson, K. Esbensen, H. Grahn, *Trends Anal. Chem.* **1992**, *11*, 41.
[14] A. Benninghoven, F. G. Rüdenauer, H. W. Werner, *Secondary Ion Mass Spectrometry*, Wiley, Chichester, 1987.
[15] H. Hutter, M. Grasserbauer, *Mikrochim. Acta* **1992**, *107*, 137.
[16] D. Böhmig, M. Reichl, *Fresenius Z. Anal. Chem.* **1993**, *346*, 223.
[17] R. C. Gonzales, P. Wintz, *Digital Image Processing*, Addison Wesley, Massachusetts, 1977.
[18] W. K. Pratt, *Digital Image Processing*, Wiley, New York, 1978.
[19] M. M. El Gomati, D. C. Peacock, M. Prutton, C. G. Walker, *J. Microsc.* **1987**, *147*, 149.
[20] D. S. Bright, D. E. Newbury, R. B. Marinenko, *Microbeam Anal.* **1988**, *23*, 18.
[21] M. Prutton, M. M. El Gomati, P. G. Kenny, *J. Electron Spectrosc. Relat. Phenom.* **1990**, *52*, 197.
[22] I. R. Barkshire, M. M. El Gomati, J. C. Greenwood, P. G. Kenny, M. Prutton, R. H. Roberts, *Surf. Interface Anal.* **1991**, *17*, 203.
[23] D. E. Newbury, D. S. Bright, in: *Secondary Ion Mass Spectrometry (SIMS VII)* (A. Benninghoven, C. A. Evans, K. D. McKeegan, H. A. Storms, H. W. Werner, eds.), Wiley, New York, 1990, pp. 929–933.
[24] D. S. Bright, D. E. Newbury, *Anal. Chem.* **1991**, *63*, 243A.
[25] P. Haberäcker, *Digitale Bildverarbeitung, 3rd Ed.*, Hanser, Wien, 1989, 255.
[26] T. Pavlidis, *Algorithms for Graphics and Image Processing*, Springer, Berlin 1982.
[27] P. Geladi, H. Grahn, K. Esbensen, E. Bengtsson, *Trends Anal. Chem.* **1992**, *11(3)*, 121–130.

Received December 29, 1994. Revision March 31, 1995.